Multivariate Polarimetric Bistatic Clutter Statistical Analysis

Carotenuto, V.; Aubry, A. ; De Maio, A. ; Fioranelli, Francesco

DOI
10.1109/RadarConf2248738.2022.9764239

Publication date
2022

Document Version
Final published version

Published in
2022 IEEE Radar Conference (RadarConf22) Proceedings

Multivariate Polarimetric Bistatic Clutter Statistical Analysis

V. Carotenuto, A. Aubry, A. De Maio
Department of Electrical Engineering and Information Technology
University of Naples Federico II, Italy
{vincenzo.carotenuto,augusto.aubry,ademaio}@unina.it

F. Fioranelli
Department of Microelectronics
Delft University of Technology, The Netherlands
f.fioranelli@tudelft.nl

***Abstract*—This paper deals with the analysis of simultaneously collected co- and cross-polarized bistatic sea-clutter returns with special emphasis on their representation as a Spherically Invariant Random Process (SIRP). The study is conducted by using appropriate testing procedures involving the complex envelope of the measured data that provide both first- and higher-order compatibility conditions. The results highlight that the SIRP model is a good candidate for the representation of bistatic coherent clutter, and usually the coherence time of the SIRP texture is longer than that in the monostatic case.**

I. Introduction

Many adaptive radar signal processing schemes (especially those focused on detection) require a preliminary statistical inference on the environment surrounding the radar. Deviations between the design and the actual clutter statistical properties may cause considerable performance degradation of the algorithm. This is particularly true for high range resolution systems possibly operating at low grazing angles where, due to the impulsive behavior of the clutter, the Gaussian model is no longer appropriate for the statistical characterization of the radar returns [1]–[7].

During the past decades, the problem of identifying suitable statistical models for sea-clutter has attracted the interest of many scientists. In this respect, based on experimental evidence on measurements collected by radar systems operating in a monostatic configuration, a widely recognized statistical framework to describe sea-clutter relies on the use of compound Gaussian (CG) distributions [1]–[5]. This is tantamount to representing the clutter backscattering as the product of two statistically independent stochastic processes commonly referred to as texture and speckle that account for macroscopic and microscopic behaviours of the sea surface, respectively. Besides, if the texture stochastic process can be approximated as a random variable over an appropriate time interval (referred to as the coherence time), then the CG model boils down to a Spherically Invariant Random Process (SIRP) [2], namely a zero-mean Gaussian process with a stochastic variance.

The work of A. Aubry and A. De Maio was partially supported by the research project SCN_00393 "S4E - Sistemi di sicurezza e protezione per l'Ambiente Mare". The work of V. Carotenuto was supported by the research program PON R&I AIM1878982-1. The authors are grateful to University College London and University of Cape Town for the provision of the data.

For radars operating in multistatic/bistatic configuration, due to the so called clutter diversity [8], namely the variation of the sea-clutter features with respect to the acquisition geometry, sea state, antenna polarization used at transmit/receive side (just to mention a few), makes the study more difficult and challenging. In this respect, an important instrument to foster a better understanding of the bistatic sea-clutter diversity as well as to characterize the differences between monostatic and bistatic clutter echoes is represented by the netted radar (NetRAD) system [9], developed from a joint collaboration between the University College London (UCL) and the University of Cape Town (UCT). NetRAD enabled the simultaneous collection of both monostatic and bistatic sea-clutter returns under different acquisition geometries and diverse polarizations for the active and passive sensors. Exploiting the measurements collected by NetRAD, relevant bistatic sea-clutter characteristics, such as radar cross section, amplitude statistics, Doppler spectra, and data correlation properties have been assessed in the open literature [9]–[17].

The statistical studies from the open literature largely focus on first-order statistics (clutter amplitude) and/or Doppler spectrum inferences. As such, a higher order statistical analysis of multistatic/multipolarimetric sea-clutter returns using the complex envelope of the available data is not yet present. This is undoubtedly of primary concern for the development of multivariate data models necessary for the radar detector design process. Besides, it may corroborate the already experimentally observed clutter diversity features.

Within this frame of reference, the goal of this paper is to fill the mentioned gap and to assess the compatibility of simultaneously collected co- and cross-polarized multistatic sea-clutter returns with the SIRP model using the complex envelope of the available data. More in detail, necessary conditions for the data to comply with the SIRP representation are tested via the Kolmogorov-Smirnov (KS) test [18], which allows to assess the goodness-of-fit between an empirical and a theoretical distribution. Both first- and Higher-Order Statistics (HOS) are considered involving also the representation of an L-dimensional data vector in terms of Generalized Spherical Coordinates (GSC). Moreover, a Cramer-Von Mises (CV) test [18] is exploited to study the local Gaussian behavior of the sea-clutter and to get estimates of the coherence time. Last but not least, a study on the spatial heterogeneity of the sea-clutter

2022 IEEE Radar Conference (RadarConf22) | 978-1-7281-5368-1/22/$31.00 ©2022 IEEE | DOI: 10.1109/RADARCONF2248738.2022.9764239

TABLE I
RADAR PARAMETERS.

Parameter	Value
Carrier Frequency	2.4 GHz
Peak Power	450 W
Modulation	Linear up-chirp
Pulse Bandwidth	45 MHz
Pulse Duration	1.8-3 μs
Pulse Repetition Frequency	1 kHz
Antenna Gain	24 dBi
Antenna Beamwidth	10° (azimuth/elevation)
Baseline	1830 m

as well as on the texture correlation among cross-channels is conducted.

The obtained results highlight that the SIRP model is a good candidate for the representation of bistatic coherent clutter and usually the coherence time of the SIRP texture is longer than that in the monostatic case.

The remainder of this paper is organized as follows. Section II briefly describes the radar system and the geometry used to collect the data. In Section III, the signal processing tools adopted to learn bistatic sea-clutter returns statistical properties are introduced. In Section IV, the aggregate results of the conducted analysis are discussed. Finally, in Section V conclusions are drawn and possible future research avenues pointed out.

II. NETRAD SYSTEM AND DATASET DESCRIPTION

NetRAD is a S-band ground-based multistatic polarimetric radar allowing the simultaneous collection of both monostatic and bistatic returns, in which, the active and passive nodes, were synchronized using GPS disciplined oscillators (GPSDOs) thus avoiding cabled connections and granting more degrees of freedom in terms of baselines among nodes.

Data exploited in this paper were collected using NetRAD on June 9th 2011 in South Africa at Misty Cliffs using three nodes: one active (with transmit and receive capabilities) and two passive [16]. The passive nodes were co-located and used to measure the bistatic sea-clutter returns from both the horizontal and the vertical polarization. Additionally, they were separated from the active sensor via a baseline of 1830 m. As to the active node, it was a pulsed radar operating over a carrier frequency of 2.4 GHz, transmitting linear up-chirp waveforms with a swept bandwidth of 45 MHz (i.e., a range resolution of 3.3 m), and a Pulse Repetition Frequency (PRF) equal to 1 kHz. For each experiment, the pulse duration was changed from 1.8 to 3 μs depending on the acquisition geometry (bistatic angle, β). Finally, the antennas used for both the active and passive nodes had approximately 24 dBi gain and 10° beamwidth both in azimuth and elevation. Table I summarizes the main parameters involved into the considered measurement campaign.

As to the acquisition geometry, the experiment was conducted on the west side of the Cape Peninsula with the sensors facing the Atlantic Ocean. As shown in Figure 1, the antennas were steered so that the intersection point between

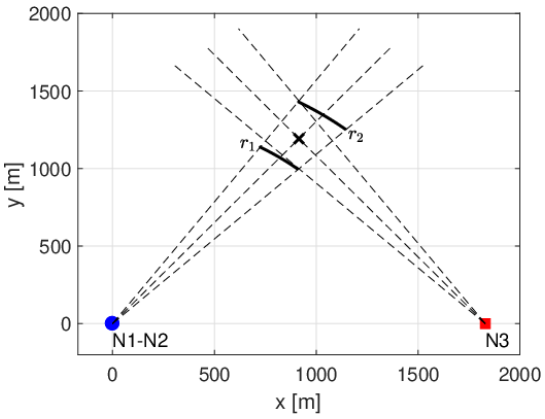

Fig. 1. System geometry for $\beta = 75°$. N3 represents the monostatic node, N1-N2 are the two co-located bistatic sensors.

the boresight of the transmitting/receiving antennas ($\times$-marked point) and the position of the nodes ($\circ$- and $\square$-marked points) occupy the vertices of an isosceles triangle with axis of symmetry perpendicular to the baseline between the two co-located passive nodes (N1-N2) and the monostatic sensor (N3). The passive nodes N1 and N2 collected data from the H and V polarization, respectively.

Different bistatic angles equal to 60°, 75°, 90°, 95°, 105°, and 120°, were considered by pointing the antennas at the transmit and the receive sides to a common clutter patch, which corresponds to the area where transmitter and receiver antenna patterns intersect. In particular, owing to the acquisition setup symmetries (both in terms of geometry and Tx-Rx radiation patterns) the minimum and maximum distance r_1 and r_2 of the clutter patch from N1 and N2 can be computed as [17]

$$\begin{aligned} r_1 &= (\delta_B/2)\cos(\theta_{3dB}/2)\,/\cos(\theta_1 - \theta_{3dB}/2)\,, \\ r_2 &= (\delta_B/2)\cos(\theta_{3dB}/2)\,/\cos(\theta_1 + \theta_{3dB}/2)\,, \end{aligned} \tag{1}$$

where δ_B denotes the baseline, θ_{3dB} is the angular width of the antenna's main lobe in azimuth, and θ_1 is the pointing angle in the azimuth direction. Notably, $[r_1, r_2]$ also identifies the monostatic, i.e., with respect to N3, range swath of the clutter patch of interest.

Table II summarizes the polarization configurations associated with each dataset along with the corresponding pulse duration of the waveform transmitted by N3. For all the mentioned acquisition scenarios, measurements refer to a time span of 130 s which, with a PRF of 1 kHz, corresponds to $N_s = 130000$ slow-time samples for each range cell. Thus, for a specific range bin, the baseband complex envelope of the bistatic sea-clutter returns for the dth dataset, $d \in D = \{1, 2, 4, 5, 6, 7, 8, 9, 11, 12, 13, 14\}$, at the sensor i, $i = 1, 2, 3$, can be expressed as

$$z_{d,i}(n) = z^I_{d,i}(n) + j z^Q_{d,i}(n), \quad n = 1, \ldots, N_s, \tag{2}$$

where $z^I_{d,i}(n)$ and $z^Q_{d,i}(n)$ denote the in-phase (I) and quadrature (Q) components, respectively. Finally, as to the environmental conditions, the wind speed/direction and wave

TABLE II
POLARIZATION CONFIGURATIONS FOR THE AVAILABLE MEASUREMENTS.

Dataset number	N3 Pol. (Tx-Rx)	N1 Pol. (Rx)	N2 Pol. (Rx)	β [deg]	Pulse Duration [μs]
1	HH	H	V	60	3
2	HH	H	V	75	3
4	HH	H	V	90	2.2
5	HH	H	V	95	2.2
6	HH	H	V	105	1.8
7	HH	H	V	120	1.8
8	VH	H	V	60	3
9	VH	H	V	75	3
11	VH	H	V	90	2.2
12	VH	H	V	95	2.2
13	VH	H	V	105	1.8
14	VH	H	V	120	1.8

height/direction remained almost constant during the experiments. Specifically, the wind speed was about 8-9 m/s blowing from the South-South-East direction, whereas the wave height and direction were $\approx$ 2 m (sea state 4) and $\approx 225^\circ$ with respect to the True North, respectively.

Before proceeding with data analysis, in the next sub-section some pre-processing operations performed on the available sea-clutter returns are described.

A. Signal Conditioning

As discussed in the previous section, the synchronization of the sensors in the NetRAD system is realized using three GPSDOs. Since these oscillators are independent, there could be differences both in terms of start triggers and oscillation frequencies. Such undesired effects lead to range misalignments and deviations of the relative phase between the signals collected at the different nodes. Both the issues are accounted for by exploiting the sidelobe-to-sidelobe direct signal, i.e., the signal in line-of-sight transmitted through the sidelobes of the transmit antenna and received through the sidelobes of the antenna at the bistatic sensors [9]. Finally, after compensating the mentioned undesired effects, DC offset (of both I and Q component) and possible imbalance between the quadrature channels are removed according to the procedure specified in [19] and [4].

III. COMPATIBILITY WITH THE SIRP MODEL

Let us denote by $z_{d,i}(t)$, $d \in D$, $i = 1, 2, 3$, the continuous-time version of (2). If this signal complies with the CG model, then it can be represented as the product of two statistically independent stochastic processes, namely as

$$z_{d,i}(t) = s_{d,i}(t) g_{d,i}(t), \quad d \in D,\ i = 1, 2, 3, \tag{3}$$

where $s_{d,i}(t)$ is a slowly varying nonnegative component and $g_{d,i}(t)$ is a zero-mean complex circular Gaussian process. They are commonly referred to, in the open literature, as texture and speckle, respectively. Interestingly, if the texture stochastic process can be approximated as a random variable. over an appropriate time interval T_c, referred to as the coherence time, the CG model in (3) boils down to

$$z_{d,i}(t) = s_{d,i} g_{d,i}(t), \quad d \in D,\ i = 1, 2, 3,\ t \in T_c, \tag{4}$$

which is a SIRP [2]. As a consequence, a finite set of samples from (4) can be stacked to form a Spherically Invariant Random Vector (SIRV), and the compatibility of the sea-clutter from a given range cell with the SIRP model can be assessed by studying the adherence of the aforementioned random vectors with the SIRV model.

Following the methodology proposed in [4], this task is accomplished using the complex envelope of the available sea-clutter data. In this respect, for a given range bin, both first-order and higher-order statistical tests have been implemented as explained in the following sub-sections along with some illustrative examples related to the measurements from set 1.

A. First-Order Statistics

Let us observe that if the available data fits the SIRV model, the ratio between the quadrature components has to follow a standard Cauchy distribution [4]. Hence, a necessary requirement for the complex envelope to comply with the SIRP model is provided by the following hypotheses

$$\begin{aligned} H_0 : R_{d,i}(n) &= \frac{z^I_{d,i}(n)}{z^Q_{d,i}(n)} \sim \mathcal{C}(0,1), \\ H_0 : \bar{R}_{d,i}(n) &= \frac{z^Q_{d,i}(n)}{z^I_{d,i}(n)} \sim \mathcal{C}(0,1), \end{aligned} \tag{5}$$

$d \in D$, $i = 1, 2, 3$, $n = 1, \ldots, N_s$, where $\mathcal{C}(0,1)$ denotes a random variable distributed according to a standard Cauchy. Besides, if the complex envelope is a SIRP, then it must comply with the circular symmetry property, i.e., the amplitude and the phase of the collected signal samples must be statistically independent, with the phase following a uniform distribution over the interval $(0, 2\pi)$. Hence, a further evidence on the compatibility of sea-clutter returns with the SIRP model can be obtained by testing the following simple hypothesis

$$H_0 :\ \phi_{d,i}(n) = \text{atan}_{IV}\left[\frac{z^Q_{d,i}(n)}{z^I_{d,i}(n)}\right] \sim \mathcal{U}(0, 2\pi), \tag{6}$$

$d \in D$, $i = 1, 2, 3$, $n = 1, \ldots, N_s$, where $\mathcal{U}(a, b)$ denotes a random variable uniformly distributed within the interval (a, b), and $\text{atan}_{IV}(\cdot)$ is the four-quadrant inverse tangent function [4]. Moreover, let us observe that if $\phi_{d,i} \sim \mathcal{U}(0, 2\pi)$, $d \in D$, $i = 1, 2, 3$, then the corresponding kurtosis and skewness are -1.2 and 0, respectively. As a consequence, to further corroborate the adherence of the phase signal with the uniform distribution, it is also possible to verify that the corresponding kurtosis and skewness agree with the expected theoretical values.

Requirements in (5) and (6) can be studied resorting to the Kolmogorov-Smirnov (KS) test [18] that allows to assess the goodness-of-fit between the empirical distribution with the corresponding theoretical counterparts. However, KS test requires independent observations. Thus, before evaluating the KS statistics, the available sea-clutter returns have been decimated in the slow-time domain to ensure almost uncorrelated, and hopefully independent, speckles for both the I and Q

TABLE III
PERCENTAGE OF RANGE BINS FOR DATASET 1 WHERE USING FIRST-ORDER STATISTICS THE SIRP ASSUMPTION CANNOT BE REJECTED FOR A 0.01 SIGNIFICANCE LEVEL.

Test	N1	N2	N3
R	100	98	99
$\bar{R}$	99	98	98
ϕ	100	100	99
$R \wedge \bar{R} \wedge \phi$	99	98	97

components. The decimation factor has been set according to the estimated decorrelation time of 0.05 s. Thus, for each range bin belonging to the clutter patch, 2600 samples have been used to evaluate the KS statistics. For all the considered datasets, the decimation process ensures an average one-lag correlation coefficient of the analyzed data smaller than 0.2.

Let us observe that to make inference on the compliance of the sea-clutter returns associated to a specific range bin with the SIRP model, both the null hypotheses in (5) and (6) have to be fulfilled. In this respect, Table III reports the percentage of range bins for which, at a 0.01 significance level, the considered null hypotheses cannot be rejected. Precisely, the first three rows refer to $R_{1,i}$, $\bar{R}_{1,i}$, and $\phi_{1,i}$, $i = 1, 2, 3$, whereas the last one reports the percentage of range bins where the first-order compatibility hypothesis cannot be rejected for any of the three aforementioned tests[1]. Table III shows that for dataset 1, and according to the considered first-order statistics, most of the sea-clutter returns for both monostatic and bistatic acquisitions exhibit a good first-order agreement with the SIRP model.

B. Higher-Order Statistics

To formulate higher-order necessary conditions about the compliance of the available data with the SIRP model it is possible to exploit the representation of a real-valued SIRV in terms of GSC. Moreover, it is also of primary concern to estimate the time scale where the texture can be approximated as a random constant.

1) GSC: Let us preliminary observe that if $\boldsymbol{x} = [x_1, \ldots, x_L]^T$ is an L-dimensional real-valued zero-mean SIRV with identity covariance matrix, assuming $L = 5$ (this is not a limitation but coincides with the value assumed for the subsequent analysis) its GSC $(R, \varphi_1, \varphi_2, \ldots, \varphi_4)$ are related to the rectangular ones through the equations

$$\begin{aligned} &R = \|\boldsymbol{x}\|, \\ &\varphi_1 = \cos^{-1}\left(\frac{x_5}{R}\right), \quad \varphi_2 = \cos^{-1}\left(\frac{x_4}{\sqrt{R^2 - x_5^2}}\right), \\ &\varphi_3 = \cos^{-1}\left(\frac{x_3}{\sqrt{R^2 - x_5^2 - x_4^2}}\right) \\ &\varphi_4 = \operatorname{sign}(x_1)\cos^{-1}\left(\frac{x_2}{\sqrt{R^2 - x_5^2 - x_4^2 - x_3^2}}\right) + \\ &\qquad\qquad - \pi\left(\operatorname{sign}(x_1) - 1\right). \end{aligned} \tag{7}$$

[1]The symbol $\wedge$ represents the logical AND operation.

TABLE IV
PERCENTAGE OF RANGE BINS FOR DATASET 1 WHERE USING HIGHER-ORDER STATISTICS THE SIRP ASSUMPTION CANNOT BE REJECTED FOR A 0.01 SIGNIFICANCE LEVEL.

Test	N1	N2	N3
φ_1	99	98	99
φ_2	99	98	99
φ_3	99	99	99
φ_4	100	99	99
$\varphi_1 \wedge \varphi_2 \wedge \varphi_3 \wedge \varphi_4$	98	95	96

Besides, the angular coordinates φ_k, $k = 1, \ldots, 4$, are independent of each other as well as of the radius R, and their CDFs (Cumulative Distribution Functions) are given by

$$\begin{aligned} &F_{\varphi_1}(\eta) = \frac{3}{4}\left(\frac{1}{3}\cos^3\eta - \cos\eta + \frac{2}{3}\right), \quad 0 \le \eta \le \pi, \\ &F_{\varphi_2}(\eta) = \frac{1}{\pi}\left(\eta - \sin\eta\cos\eta\right), \quad 0 \le \eta \le \pi, \\ &F_{\varphi_3}(\eta) = \frac{1}{2}\left(1 - \cos\eta\right), \quad 0 \le \eta \le \pi, \\ &F_{\varphi_4}(\eta) = \frac{1}{2\pi}\eta, \quad 0 \le \eta \le 2\pi. \end{aligned} \tag{8}$$

Accordingly, for a given dataset and node, using the I or Q component of the collected samples, segmenting them in sub-vectors of length 5, and evaluating $\varphi_1, \ldots, \varphi_4$, via (7), the compatibility with the SIRV model can be analyzed. Specifically, multiple KS tests can be performed to assess the goodness-of-fit between the empirical distributions of the phases associated with the generalized spherical representation and their theoretical counterparts in (8). This is tantamount to jointly testing the simple hypotheses

$$H_{0,k} : \varphi_{d,k,i} \text{ has the CDF } F_{\varphi_{k,d,i}}, \quad k = 1, \ldots, 4 \tag{9}$$

where $\varphi_{d,k,i}$ is the kth, $k = 1, \ldots, 4$, angular coordinate associated with the dataset d and the sensor node i, $d \in D$ and $i = 1, 2, 3$. Each of the hypotheses in (9) represents a necessary condition for the data vector to be modelled as a SIRV. In this respect, Table IV reports the percentage of range bins for which the SIRV hypothesis cannot be rejected, assuming a significance level of 0.01 for each angular coordinate test. Specifically, the first four rows refer to the results obtained testing each of the hypotheses $H_{0,k}$, $k = 1, \ldots, 4$, whereas the last refers to the percentage of range bins where all the four hypotheses cannot be rejected. The results show that for both the bistatic and the monostatic measurements there is an overall compliance of the sea-clutter returns with the SIRV model. Since both first- and higher-order statistics represent necessary requirements for the compliance of the sea-clutter returns with the SIRP model, using both first- and higher-order statistics the overall percentage of range bins agreeing with the SIRP model (evaluated considering $R \wedge \bar{R} \wedge \phi \wedge \varphi_1 \wedge \varphi_2 \wedge \varphi_3 \wedge \varphi_4$) is 97% for N1, 93% for N2, and 93% for N3.

2) Coherence Time: As already highlighted, the SIRP model represents a valuable description of the CG process within the coherence time T_c, i.e., the temporal interval where the texture component can be modelled as a random

variable. Over such temporal scale, the clutter exhibits a local Gaussian behaviour, namely the received data (under the SIRP assumption) can be deemed as a zero-mean complex circular Gaussian process with unknown variance. This observation paves the way to the design of an effective strategy to estimate T_c. Specifically, T_c can be inferred from the available measurements by considering data sequences of increasing length (from both the quadrature components) and establishing whether the following hypothesis can not be rejected

$$H_{0,n} : \mathcal{P}\{z_{d,i}(t)\} \sim \mathcal{N}(0, \sigma_g^2), \quad t \in [0, T_n], \; n = 1, \ldots, N, \tag{10}$$

$d \in D$, $i = 1, 2, 3$, where $\mathcal{P}(\cdot)$ denotes either the real or the imaginary part of the argument, $\mathcal{N}(0, \sigma_g^2)$ denotes a zero-mean Gaussian random variable with variance σ_g^2, T_n is the temporal-duration of the nth sequence under test, σ_g^2 is the unknown variance parameter, and N is the total number of considered data sequences. In particular, T_n is progressively increased by 1.25 s, i.e., $T_n = n1.25$ s, $n = 1, \ldots, N$. Since the available data have been collected over a time span of 130 s, the total number of analyzed sequences is equal to 104. Besides, considering the decimation factor of 50 samples which, as discussed in Section III-A, ensures almost uncorrelated and hopefully almost independent speckle components, and the value of PRI, the shortest analyzed sequence (i.e., T_1) corresponds to 25 samples.

For each range bin of a specific dataset, the hypotheses $H_{0,n}$, $n = 1, \ldots, N$, can be tested by applying progressively the Cramer-Von Mises (CV) test [18] to the data belonging to the temporal interval $[0, T_n]$, $n = 1, \ldots, N$. It is expected that when the observation period becomes greater than the coherence length of the sequence, $H_{0,n}$ should be rejected and the texture component could be no longer modelled as a constant value.

Using the measurements from dataset 1, Figures 2(a) and 2(b) show the CV-distances versus the length of the analyzed temporal segments evaluated using the I and the Q components, respectively. Precisely, the reported CV distances have been averaged over the range bins belonging to the clutter patch for which both first- and higher-order statistics comply with the SIRP model with a significance level of 0.01. Comparing the obtained results with the threshold at 0.01 significance level, it is possible to estimate the coherence time as the smallest T_n where the average CV distance exceeds the threshold, i.e., as the temporal-length after which the local Gaussian hypothesis has to be rejected. For the considered dataset, the plots point out that the estimated coherence time for the monostatic measurements is much smaller than the bistatic counterparts. Specifically, considering the measurements collected by N3 and N1, the estimated average coherence time (over the quadrature components) is about 6 s and 34 s, respectively. As to the cross-polarized signals, the □-marked blue curves of Figures 2(a) and 2(b) reveal that the local Gaussian assumption can not be rejected for the whole acquisition time. To the best of the authors' knowledge, this is a new and important achievement in the context of bistatic clutter characterization, which further sheds lights on the concept of clutter diversity [8].

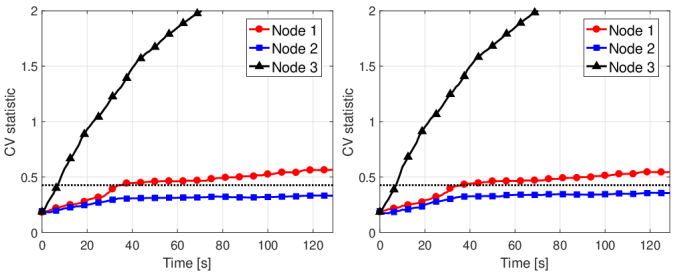

Fig. 2. Average coherence time evaluated over the I (a) and Q (b) components for dataset 1.

TABLE V
PERCENTAGE OF RANGE BINS WHERE, USING BOTH FIRST- AND HIGHER-ORDER STATISTICS, THE COMPLIANCE WITH THE SIRP MODEL CANNOT BE REJECTED WITH A SIGNIFICANCE LEVEL OF 0.01.

Dataset	β	N1	N2	N3
1	60°	97	93	93
2	75°	N/A	N/A	N/A
4	90°	97	93	88
5	95°	98	90	93
6	105°	79	94	98
7	120°	91	97	94
8	60°	92	96	95
9	75°	94	97	92
11	90°	94	99	94
12	95°	95	98	89
13	105°	100	98	96
14	120°	100	36	91

IV. AGGREGATE RESULTS

In this section, the statistical tools presented in Section III to establish the adherence of the sea-clutter radar returns with the SIRP model are applied to all the available datasets in order to provide aggregate results.

As a first analysis, Table V reports for each dataset the percentage of range bins where both first- and higher-order statistics suggest the compatibility of the observed clutter returns with the SIRP model. The percentages are computed evaluating the number of range cells where the null hypotheses in (5), (6), and (9), cannot be rejected with a 0.01 significance level. Note that measurements from dataset 2 are not considered because the data acquired by at least one of the three nodes was collected over a time window shorter than 130 s. This is the reason why the mentioned dataset is marked as Not/Analyzed (N/A).

Regardless the considered acquisition setup, the results highlight a good agreement between the monostatic sea-clutter returns and the SIRP model. As to the bistatic returns, the percentage of range bins where the compliance with the SIRP model cannot be rejected depends on both the polarization configuration and the bistatic angle. Table V shows that, except for the co-polarized bistatic measurements of datasets 6 and 14, both the available monostatic and bistatic data adhere well with a SIRP representation.

TABLE VI
AVERAGE COHERENCE TIME EVALUATED USING BOTH THE QUADRATURE COMPONENTS.

		N1			N2			N3		
Dataset	β [deg]	c_I [s]	c_Q [s]	c_{IQ} [s]	c_I [s]	c_Q [s]	c_{IQ} [s]	c_I [s]	c_Q [s]	c_{IQ} [s]
1	60°	35.0	36.3	35.6	0.0	0.0	0.0	7.5	7.5	7.5
2	75°	N/A	N/A	N/A	N/A	N/A	N/A	N/A	N/A	N/A
4	90°	22.5	27.5	25.0	35.0	35.0	35.0	5.0	3.8	4.4
5	95°	22.5	21.3	21.9	23.8	25.0	24.4	7.5	6.3	6.9
6	105°	12.5	11.3	11.9	12.5	13.8	13.1	6.3	6.3	6.3
7	120°	8.8	12.5	10.6	16.3	17.5	16.9	8.8	8.8	8.8
8	60°	0.0	0.0	0.0	33.8	31.3	32.5	12.5	12.5	12.5
9	75°	68.8	71.3	70.0	15.0	15.0	15.0	8.8	8.8	8.8
11	90°	77.5	76.3	76.9	52.5	50.0	51.3	10.0	10.0	10.0
12	95°	38.8	36.3	37.5	17.5	18.8	18.1	11.3	11.3	11.3
13	105°	12.5	12.5	12.5	8.8	8.8	8.8	15.0	12.5	13.8
14	120°	8.8	8.8	8.8	5.0	1.3	3.1	11.3	12.5	11.9

The next analysis is focused on the estimation of the coherence time. Table VI summarizes the results for all the considered datasets where c_I and c_Q indicate the coherence time estimated using the I and Q component, respectively, whereas c_{IQ} is the corresponding average. By analyzing the reported values, the following consideration can be drawn

- for each dataset, c_I and c_Q almost coincide;
- for both the horizontal and vertical co-polarized scenarios, at the passive side the estimated coherence time is smaller than the cross-polarized counterparts;
- the measurements collected by N1 in co-polarized mode exhibit a coherence time that decreases as the bistatic angle increases;
- for $\beta = 60^\circ$ and cross-polarized bistatic sensing, the textures associated with the data acquired by N1 and N2 can be well approximated with a constant but unknown value over the whole acquisition interval;
- using the vertical polarization at the active node, for $\beta = 105^\circ$ and 120° the bistatic cross-polarized returns at N1 exhibit a coherence time smaller than the monostatic one.

V. CONCLUSIONS

This paper has considered the statistical analysis of sea-clutter returns collected via a bistatic radar configuration with different transmit and receive polarizations. The study has been focused on establishing the agreement between the available measurements and the SIRP representation. To this end specific statistical procedures based on KS and CV tests have been used. The analysis has highlighted a good level of SIRP compatibility with a coherence time usually longer than the value measured by a simultaneously operating monostatic system. Possible future researches can leverage the aforementioned statistical characterization and design suitable algorithms for joint bistatic/monostatic radar detection of targets embedded in sea-clutter.

REFERENCES

[1] K. Ward, "Compound representation of high resolution sea clutter," *Electronics Letters*, vol. 17, pp. 561–563(2), August 1981.

[2] E. Conte and M. Longo, "Characterisation of radar clutter as a spherically invariant random process," *IEE Proceedings F (Communications, Radar and Signal Processing)*, vol. 134, pp. 191–197, April 1987.

[3] A. Farina, F. Gini, M. Greco, and L. Verrazzani, "High resolution sea clutter data: statistical analysis of recorded live data," *IEE Proceedings - Radar, Sonar and Navigation*, vol. 144, pp. 121–130(9), June 1997.

[4] E. Conte, A. De Maio, and C. Galdi, "Statistical analysis of real clutter at different range resolutions," *IEEE Transactions on Aerospace and Electronic Systems*, vol. 40, no. 3, pp. 903–918, 2004.

[5] J. Carretero-Moya, J. Gismero-Menoyo, A. Blanco-del Campo, and A. Asensio-Lopez, "Statistical analysis of a high-resolution sea-clutter database," *IEEE Transactions on Geoscience and Remote Sensing*, vol. 48, no. 4, pp. 2024–2037, 2010.

[6] V. Duk, D. Cristallini, P. Wojaczek, and D. W. OHagan, "Statistical analysis of clutter for passive radar on an airborne platform," in *2019 International Radar Conference (RADAR)*, 2019, pp. 1–6.

[7] L. Rosenberg and V. Duk, "Land clutter statistics from an airborne passive bistatic radar," *IEEE Transactions on Geoscience and Remote Sensing*, vol. 60, pp. 1–9, 2022.

[8] H. D. Griffiths, "Keynote address: clutter diversity: A new degree of freedom in multistatic radar," in *2014 IEEE Radar Conference*, 2014, pp. 11–11.

[9] W. Al-Ashwal, "Measurement and modelling of bistatic sea clutter," Ph.D. dissertation, University College London, London, U.K., 2011.

[10] H. Griffiths, "Developments in bistatic and networked radar," in *Proceedings of 2011 IEEE CIE International Conference on Radar*, vol. 1, 2011, pp. 10–13.

[11] M. A. Ritchie, W. A. Al-Ashwal, A. G. Stove, K. Woodbridge, and H. D. Griffiths, "Coherent analysis of horizontally-polarized monostatic and bistatic sea clutter," in *IET International Conference on Radar Systems (Radar 2012)*, 2012, pp. 1–5.

[12] W. A. Al-Ashwal, K. Woodbridge, and H. D. Griffiths, "Analysis of bistatic sea clutter - part i: Average reflectivity," *IEEE Transactions on Aerospace and Electronic Systems*, vol. 50, no. 2, pp. 1283–1292, 2014.

[13] ——, "Analysis of bistatic sea clutter - part ii: Amplitude statistics," *IEEE Transactions on Aerospace and Electronic Systems*, vol. 50, no. 2, pp. 1293–1303, 2014.

[14] R. Palamà, M. S. Greco, P. Stinco, and F. Gini, "Statistical analysis of bistatic and monostatic sea clutter," *IEEE Transactions on Aerospace and Electronic Systems*, vol. 51, no. 4, pp. 3036–3054, 2015.

[15] M. Ritchie, A. Stove, K. Woodbridge, and H. Griffiths, "Netrad: Monostatic and bistatic sea clutter texture and doppler spectra characterization at s-band," *IEEE Transactions on Geoscience and Remote Sensing*, vol. 54, no. 9, pp. 5533–5543, 2016.

[16] F. Fioranelli, M. Ritchie, H. Griffiths, S. Sandenbergh, and M. Inggs, "Analysis of polarimetric bistatic sea clutter using the netrad radar system," *IET Radar, Sonar & Navigation*, vol. 10, no. 8, pp. 1356–1366, 2016.

[17] L. Rosenberg, S. Watts, and M. S. Greco, "Modeling the statistics of microwave radar sea clutter," *IEEE Aerospace and Electronic Systems Magazine*, vol. 34, no. 10, pp. 44–75, 2019.

[18] R. D'Agostino and M. Stephens, *Goodness-of-Fit Techniques*. New York: Marcel Dekker, 1986.

[19] J. T. Nohara, "Detection of growlers in sea clutter using an x-band pulse-doppler radar," Ph.D. dissertation, McMaster University, 1991.